Spatial and temporal patterns of remote-sensed and field-measured rainfall in southern California

Nikolay P. Nezlin and Eric D. Stein

ABSTRACT - Quantification of spatial and temporal patterns of rainfall is an important step toward developing regional hydrological models. However, traditionally used rain gauge data are sparse and do not always provide adequate spatial representation of rainfall. In this study, we evaluated remote-sensed atmospheric precipitation data as an alternative to rain gauge-measured data. We compared data from the watersheds of southern California during the period of 1996–2003, focusing on the comparison of patterns of spatial, seasonal, and interannual rainfall dynamics. We used Empirical Orthogonal Functions to discern the patterns of precipitation and atmospheric circulation at different time scales, from synoptic to interannual. The correlation between the daily rain gauge-measured and remote-sensed precipitation was poor, likely because satellite data are collected only once (or several times) a day. The resulting patterns are different than the temporal patterns of precipitation accumulated by rain gauges. We concluded that remote-sensed precipitation cannot be used to assess hydrological processes in arid zones like southern California and would not be a recommended surrogate for event-based hydrologic modeling. At the same time, the interannual variabilities of remote-sensed and gauge-measured precipitation were highly correlated and the regional patterns of gauge-measured and remote-sensed precipitation variability were similar. Therefore, remote-sensed precipitation data may be appropriate for use in long-term regional hydrologic or climate modeling. Both data sets showed that precipitation generally decreases from the northern to the southern watersheds. At interannual time-scale, the rainfall is related to the ENSO cycle. At synoptic time-scales, the rainfall patterns in southern California result from atmospheric moisture transport from the south-southwest.

INTRODUCTION

During recent years, the increased accuracy and availability of remote-sensed data has made it a viable alternative to traditionally used rain gauge data for developing regional models of rainfall, runoff, and river plume dynamics. The observations of atmospheric precipitation collected by satellites play a critical role in the monitoring of meteorological processes over the majority of the Earth's surface (Arkin and Ardanuy 1989, Huffman *et al.* 2002). The advantage of remote-sensed data over rain gauges is that they provide relatively uniform and consistent spatial and temporal coverage of rainfall information. Also, rain gauges may be less common, less densely deployed, or less consistently maintained in the open ocean and in unpopulated areas, resulting in spatial and temporal data gaps. Daily digital satellite observations of rainfall have only been widely available for the past few years, and their accuracy and application for rainfall-runoff analysis has not been statistically evaluated. Nevertheless, the remote-sensed monitoring of the environment is developing rapidly and a sufficient duration of data is available for more rigorous evaluation.

Southern California has an arid Mediterranean climate with short rainstorm events, which typically occur during winter season. The rainstorm patterns are affected by a complex combination of atmospheric circulation and topographic effects. Low-pressure winter storms typically move southward from the North Pacific along the western edge of North America. As these storm systems approach southern California, they are moderated by the Pacific high-pressure system and a thermal low to the east, which deflects many storms (Bailey 1966). As a result, the average annual rainfall in southern California is only 30–50 cm. During winter, the center of high pressure moves to a southwest position, allowing brief, intense Pacific stormfronts to penetrate the area (Lu

et al. 2003). Rainfall patterns are moderated further by a temperature inversion created by the ring of mountain ranges that define southern California. The east-west Transverse Ranges and the north-south Peninsular Ranges create a "coastal basin" where cool, dense air is trapped. This basin often deflects marine winds over the area, resulting in much weaker wind patterns than over the open ocean and lower rainfall than areas to the east (Dorman and Winant 1995). In addition to annual and seasonal atmospheric cycles, rainfall patterns are governed by atmospheric processes that operate at interannual to multi-decadal time scales, such as the El Niño Southern Oscillation (ENSO) and the Pacific Decadal Oscillation (PDO).

Understanding the variability of rainfall patterns is an important element to developing conceptual and predictive models of runoff, pollutant loading, and river plume dynamics. For example, the intensity and spatial distribution of rainfall can affect the magnitude and duration of pollutant washoff to the ocean (Tiefenthaler and Schiff 2003, Vaze and Chiew 2003). The interval between rain events, along with the characteristics of the watershed, will influence the lag time between rainfall and runoff and the portion of total precipitation that translates to surface runoff (Mount 1995, Ward and Elliot 1995, Ackerman *et al.* In press). The ability to monitor and analyze patterns and processes that control rainfall variability is critical to the accuracy of models used to support the development and evaluation of storm water management practices.

In this study, we compare the spatio-temporal rainfall patterns revealed from the analysis of remote-sensed and gauge-measured precipitation in southern California. The remote-sensed measurements of atmospheric precipitation are based on the estimated concentration of precipitable water vapor in the atmosphere rather than rainfall reaching the earth surface. Therefore, the correlation between the remote-sensed and gauge-measured data is often not high. The goal of this study is to answer the question: how well do remote-sensed measurements represent the basic features of rainfall in the study area, i.e., how confident would we be using these data in the predictive models that relate runoff and pollutant loading to climatic cycles at various spatial and temporal scales? For this, we compared daily digital satellite precipitation data to precipitation measured by standard rain gauge stations. Then, we used statistical methods to quantify spatial and temporal patterns in rainfall and wind and to compare them to global climatological cycles (e.g., ENSO and PDO). The resulting data were used to discern the effect of forcing functions operating at different time scales on regional precipitation patterns.

METHODS

Precipitation Data

Satellite and rain gauge rainfall data were collected for the period 1996 through 2003, a period during which daily satellite images for rainfall are readily available. Daily digital maps of remote-sensed precipitation, produced as a part of the Global Precipitation Climatology Project (GPCP), were obtained from the NASA Goddard Space Flight Center Distributed Active Archive Center (NASA GSFC DAAC). The data are based on (1) the measurements of Special Sensor Microwave/Imager (SSM/I) multi-channel passive microwave radiometers on Defense Meteorological Satellite Program (DMSP) satellites, (2) infrared (IR) sensors on Geosynchronous Operational Environmental Satellites (GOES, USA), (3) Geosynchronous Meteorological Satellite (GMS, Japan), (4) Meteorological Satellite (METEOSAT, European Community), (5) the NOAA-series Low-Earth-Orbit Satellite (LEO, USA), and (6) the TIROS Operational Vertical Sounder (TOVS) data. The data are derived from the High-Resolution Infrared Sounder 2 (HIRS2), Microwave Sounding Unit (MSU), and Stratospheric Sounding Unit (SSU) instruments on the NOAA series of polar orbiting meteorological satellites. The daily averaged satellite data are interpolated to a global grid of 1° spatial resolution. Data were extracted for analysis from four 1° by 1° grids covering the area located between 31°30'N and 35°30'N and 121°30'W and 115°30'W (Figure 1).

Daily rain gauge data were obtained from 98 meteorological stations located in southern California (Figure 1). The data were downloaded from the NOAA National Data Center Climate Data Online (NNDC/CDO) Internet site. Each observation represents precipitation during a 24-h period preceding the observation time. The precise time of observation differed between stations and between days; therefore, each observation was attributed to an entire day and the variability was not analyzed at a time-scale less than daily. Not all stations had continuous data for the entire 7.5-year period of analysis. To obtain the continuous time-series of precipita-

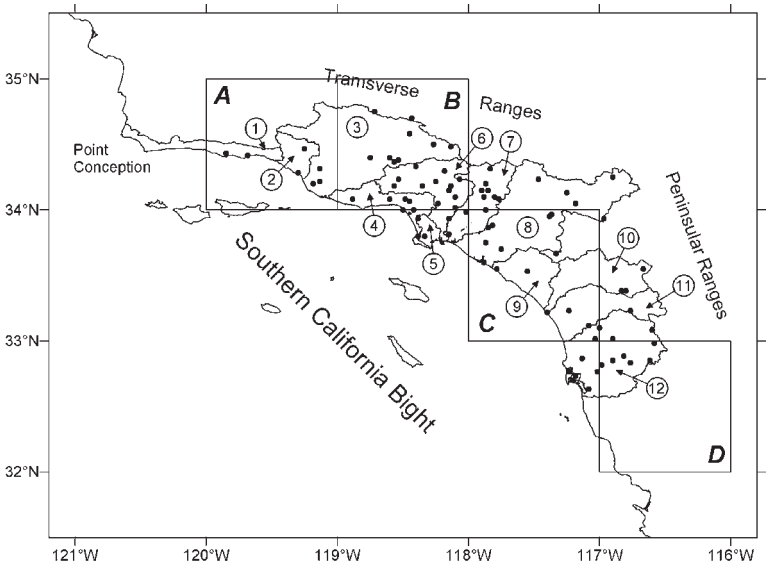

Figure 1. The map of watersheds (1-12, see Table 1) and raingage stations (solid circles) in southern California; the location of grid cells of the remote-sensed precipitation (GPCP): 34º30'N, 119º30'W (A); 34º30'N, 118º30'W (B); 33º30'N, 117º30'W (C); 32º30'N, 116º30'W (D).

tion in different parts of the study area, all stations were classified to 12 watersheds (Appendix A) and the precipitation was averaged over each watershed area.

Wind Data

Wind data were obtained from the National Center for Environmental Prediction (NCEP); the global wind data are supplied by the NASA GSFC DAAC as ancillary information for SeaWiFS users. These files contain regular grids of zonal and meridional wind speeds at 10 m above the earth surface interpolated on an equidistant cylindrical projection of 1º spatial resolution and 6-h temporal resolution (12-h during some periods in 1998 and 1999). Wind pattern was analyzed within the rectangle from 31ºN to 36ºN and from 122ºW to 115ºW during the period from March 1997 to October 2003.

Statistical Analysis

Seasonal patterns were estimated by averaging precipitation over the entire 7.5 years of observations (January 1996–June 2003) for each watershed during each day of the seasonal cycle. We used the Empirical Orthogonal Functions (EOF) method to analyze spatio-temporal variability of precipitation and wind and the relationship between the two. This statistical approach is a convenient method for analysis of the successive patterns of spatially distributed data. The EOF method (Priesendorfer 1988) decomposes space- and time-distributed data into a set of orthogonal functions (spatial maps) and the corresponding principle components (time series). Each of these orthogonal functions then is ranked by its variance. In this study, we analyze total values of precipitation and wind rather than their anomalies; therefore, we did not analyze pure spatial or temporal variance, but the joint space-time variance. The EOF method was applied to remote-sensed precipitation (2,464 daily observations during October 1st 1996–June 30th 2003 at each of 35 grid cells of the rectangle 31.5–35.5ºN; 121.5–115.5ºW), gauge-measured precipitation (2,738 daily observations during January 1st 1996–June 30th 2003 at each of 12 watersheds), and wind (8,985 observations during March 13th 1997–June 30th 2003 at each of 48 grid cell of the rectangle 31–36ºN; 122–115ºW; zonal and meridional wind components in each cell resulted in total 96 variables).

To relate the long-scale meteorological variations in southern California to the global climatic meteorological cycles, we used the NINO3 index (sea surface temperature anomalies averaged over the region 5ºS–5ºN; 150ºW–90ºW in equatorial Pacific) and the Southern Oscillation Index (SOI, the difference between the standardized measurements of the Sea Level Atmospheric Pressure in Tahiti and Darwin) obtained from the International Research Institute of Climate Prediction (Columbia University, USA).

Results

Spatial Patterns of Rainfall

The daily rainfall data measured by two methods in different locations were not highly correlated. Correlation analysis revealed that daily remote-sensed precipitation data were only moderately comparable to rain gauge data, with correlations being stronger in the northern watersheds than in the southern watersheds (Table 1). Correlation coefficients between precipitation in each watershed and in the four grid cells of the global remote-sensed precipitation map ranged from +0.17 to +0.67. Correlations were stronger based on seasonal variations (i.e., 365

Table 1. Correlation between the variations of precipitation in the watersheds of southern California and the remote-sensed precipitation in four locations during October 1996-June 2003. In parentheses correlation coefficients estimated from the seasonal patterns of precipitation (365 averaged climatic days).

		A 34°30'N, 119°30'W	B 34°30'N, 118°30'W	C 33°30'N, 117°30'W	D 32°30'N, 116°30'W
1	Santa Barbara Creek	+0.47 (+0.54)	+0.39 (+0.49)	+0.27 (+0.34)	+0.17 (+0.23)
2	Ventura River	+0.44 (+0.46)	+0.48 (+0.53)	+0.41 (+0.44)	+0.25 (+0.31)
3	Santa Clara River	+0.52 (+0.63)	+0.48 (+0.62)	+0.41 (+0.51)	+0.30 (+0.41)
4	Santa Monica Bay	+0.46 (+0.57)	+0.45 (+0.57)	+0.39 (+0.48)	+0.30 (+0.39)
5	Dominguez Channel	+0.58 (+0.67)	+0.55 (+0.66)	+0.50 (+0.58)	+0.38 (+0.47)
6	Los Angeles River	+0.46 (+0.57)	+0.46 (+0.59)	+0.42 (+0.51)	+0.33 (+0.41)
7	San Gabriel River	+0.45 (+0.51)	+0.42 (+0.53)	+0.39 (+0.47)	+0.27 (+0.35)
8	Santa Ana River	+0.41 (+0.51)	+0.46 (+0.57)	+0.41 (+0.49)	+0.26 (+0.36)
9	San Juan Creek	+0.42 (+0.50)	+0.48 (+0.55)	+0.43 (+0.47)	+0.25 (+0.32)
10	Santa Margarita River	+0.32 (+0.41)	+0.37 (+0.48)	+0.33 (+0.39)	+0.26 (+0.32)
11	San Luis Rey River/Escondido Creek	+0.27 (+0.41)	+0.31 (+0.45)	+0.30 (+0.38)	+0.24 (+0.32)
12	San Diego River	+0.37 (+0.49)	+0.41 (+0.55)	+0.38 (+0.48)	+0.32 (+0.41)

averaged climatic days) than on the basis of the entire period of observations (October 1996–June 2003). However, spatial relationships between the remote-sensed grids and the associated watersheds were weak. Correlation coefficients between a specific 1º by 1º grid cell and its corresponding watersheds were only slightly higher than those of other watersheds in the region. This is especially true for the cell that overlies the southern watersheds (Location D at Figure 1), where low correlation coefficients were comparable with all 12 watersheds. The low correlation can be attributed partly to the fact that this cell is spatially offset from the southern watersheds (see Figure 1).

The regional annual rainfall patterns revealed from remote-sensed and rain gauge data were similar, confirming the previously documented trend of decreasing precipitation from northern to southern watersheds (Tables 2-3) (Beuhler 2003). Maximum mean annual rain gauge-measured precipitation (54.8 cm/year) was observed in the northernmost Santa Barbara Creek watershed and the minimum mean annual precipitation (32.54 cm/year) occurred in the southernmost San Diego River watershed. The same north-to-south trend was apparent in the annual remote-sensed precipitation data (Figure 2 and Table 3), although the absolute values were substantially lower, from 28.4 cm/year in the north to 11.3 cm/year in the south.

Year-to-year variability of both remote-sensed and gauge-measured precipitation was very high, as is typical for Mediterranean climates (see Tables 2–3). In all cases, the maximum precipitation was observed in 1997/1998 and the minimum was in 2001/2002. In gauge-measured precipitation, the ratio between the "wettest" and the "driest" years ranged from 5.1-fold for the Santa Barbara Creek watershed to 10.7-fold for the San Gabriel River watershed. In remote-sensed precipitation, the ratio ranged from 4.9 for the northernmost watershed to 7.0 for the southernmost one (Table 3). However, no clear north-to-south pattern was observed in relative differences between wet and dry years in the gauge-measured data.

The seasonal patterns of remote-sensed and gauge-measured data precipitation are similar (Figures 3 and 4). In gauge-measured data, seasonal patterns were consistent among watersheds. The magnitude of difference between the wet and dry portions of the year generally decreased from north to south, i.e., seasonal patterns were muted in the southern watersheds (Figure 3). Rainstorms generally occur from the end of October to April of the next year, with most intensive rainstorms in February. Northern watersheds regularly experience daily mean rain gauge precipitation in excess of 2 cm, whereas in the southern watersheds it rarely exceeds 1 cm. As with the total annual precipitation, the remote-sensed data exhibit a similar pattern, but daily mean values are generally lower than those observed in the rain gauges (Figure 4).

The spatio-temporal patterns revealed by the Empirical Orthogonal Functions were similar in remote-sensed and gauge-measured precipitation. Results of the EOF analysis identified the modes that contribute to spatial variability in precipitation pat-

Table 2. Summary of rain gage data for twelve watersheds in southern California that discharge to the Pacific Ocean. Watersheds are listed from north to south.

#	Watershed	Area (km^2)	Annual raingage-measured precipitation in 1996-2003 (cm)		
			Mean	Minimum (2001/2002)	Maximum (1997/1998)
1	Santa Barbara Creek	971	54.80	23.19	119.35
2	Ventura River	696	47.33	19.19	108.66
3	Santa Clara River	5164	37.34	14.82	83.73
4	Santa Monica Bay	1170	39.46	11.59	84.86
5	Dominguez Channel	300	33.92	11.01	79.88
6	Los Angeles River	2161	48.04	16.83	108.79
7	San Gabriel River	1758	43.25	9.44	101.19
8	Santa Ana River	5101	33.85	10.68	78.93
9	San Juan Creek	1284	36.88	12.45	89.31
10	Santa Margarita River	1915	36.98	14.88	80.56
11	San Luis Rey River/Escondido Creek	2002	38.47	14.92	96.69
12	San Diego River	3561	32.54	12.34	77.58

Table 3. Annual remote-sensed precipitation (cm) in four locations (see Figure 1). Grid cells are listed from north to south.

#	Center of the 1°x1° grid cell	Annual remote-sensed precipitation in 1996-2003 (cm)		
		Mean	Minimum (2001/2002)	Maximum (1997/1998)
1	34°30'N, 119°30'W	28.44	12.52	61.62
2	34°30'N, 118°30'W	24.13	9.12	51.83
3	33°30'N, 117°30'W	16.54	5.47	37.33
4	32°30'N, 116°30'W	11.31	3.69	25.87

terns, with the first two modes accounting for 84.17% and 70.56% of the total variability in both the rain gauge and remote-sensed data, respectively (Table 4).

The first EOF modes for both data sets represent total rainstorm magnitude. In the rain gauge data, the first EOF mode accounts for 71.36% of the total variability between the 12 watersheds analyzed. Factor loadings for the first EOF mode for all 12 watersheds were positive and high, ranging from +0.66 to +0.94 (Table 5). In general, the watersheds located in the center of the study area provide maximum contribution to the total variability. For the remote-sensed precipitation data, the first EOF mode explains 58.88% of variability and its maximum is located in the center of the study area (Table 4, Figure 5A). The second EOF modes for both data sets represent the north/south variability of rainstorms over southern California (Table 4, Figure 5B); the second EOF mode explains 12.81% of the total variability of rain gauge precipitation and 11.68% of the total variability of the remote-sensed precipitation. The positive change of the second EOF mode indicates a migration of the center of a rainstorm to the south. The third EOF modes of both data sets explain only 4.25% and 6.86% of the total variability and do not exhibit a clear pattern of spatio-temporal variations; therefore, they were not analyzed further.

Relationship Between Rain and Wind Patterns

To compare the spatio-temporal patterns of precipitation derived from remote-sensed and gauge-measured observations, we analyzed the correlation between their dynamics and the patterns of wind variability in southern California.

The general pattern of wind averaged over 6.5 years of observations shows persistent northwesterly wind over the open ocean (Figure 6). Near the shore and over the land, the mean wind speed abruptly decreases and changes to a westerly direction. Results of the EOF analysis revealed the first two modes combined explained 52.34% of total spatial variability in wind patterns (Table 4). The first EOF mode coincided with the general direction of wind over southern California (from northwest to southeast over the ocean and from west to east over the

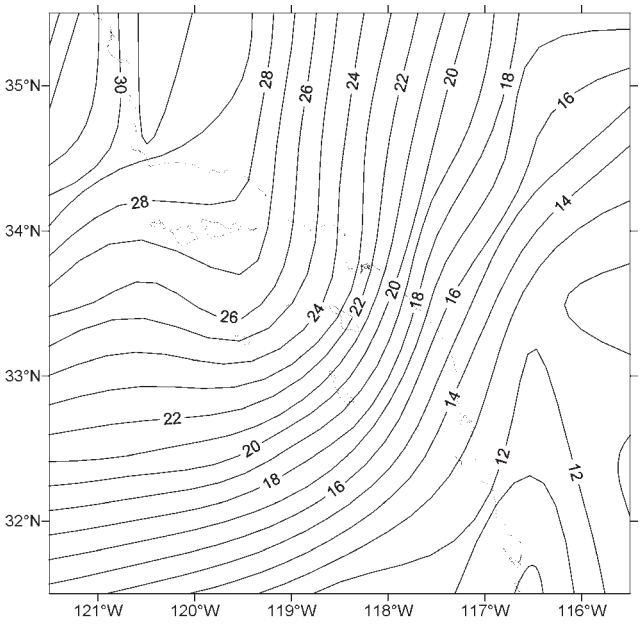

Figure 2. Precipitation contours (cm/year) based on remote-sensed data (GPCP) averaged over the period of October 1996-June 2003.

land, Figure 7A), and explained 32.78% of total variability. This mode was more pronounced over the ocean than over the land. The second EOF mode represented south-southwesterly wind patterns, and explained 19.56% of total spatio-temporal variability in wind patterns (Table 4). This mode was more pronounced over the land than over the ocean (Figure 7B). The third EOF mode explained only 8.17% of total variability, and was not analyzed further.

Wind patterns were related to the patterns of remote-sensed and gauge-measured precipitation, represented in the EOF modes in a similar way. To compare the inter-relationships between rainfall and wind patterns, cross-correlation analysis was used. This analysis compared the time-series variations of the two leading EOF modes of wind and the two leading EOF modes of rain gauge-measured and remote-sensed precipitation (Table 6, Figure 8). The first EOF mode of wind was correlated negatively with the first EOF mode of both rain-gauged and remote-sensed precipitation with a time lag 1–2 d (Figure 8A, C), meaning that a strengthening of dominating northwesterly wind results in more precipitation over the study area during the following 2 d. At the same time, the first EOF mode of wind was correlated positively with the second EOF mode of the gauge-measured precipitation with a time lag about zero, meaning that a strengthening of northwesterly wind shifts rainstorms to the southern part of the study area. The correlation between the first EOF mode of wind and the second EOF mode of remote-sensed precipitation was similar but slightly weaker.

The second EOF mode of wind was correlated positively with the first EOF mode of the gauge-measured precipitation with a small time lag (<1 d). The correlation with the second EOF mode of the gauge-measured precipitation was small; the correlation at zero time lag was inverse and changed to positive with increase of the time lag to 1–2 d (Figure 8F). These correlations indicate that strengthening of the southerly winds results in an increase of precipitation over southern California and a migration of the center of precipitation during the next 1–2 d from the south to the north. The correlations between the second EOF mode of wind and two EOF modes of the remote-sensed precipitation were small, compared to the gauge-measured precipitation.

Influence of Long-term Climatic Cycles

In contrast to daily data, the correlation between the remote-sensed and gauge-measured precipitation averaged annually during wet periods (July-June of the next year) was very high (Table 6). All coefficients exceeded +0.9 and were significant, in spite of very small data set (N=7). The gauge-measured precipitation in the southern watersheds was correlated better with the remote-sensed precipitation in all four grid cells.

Both gauge-measured and remote-sensed monthly precipitation data were subject to long-term (i.e., intra-seasonal to interannual) variations related to global weather patterns, i.e., SOI and NINO3 indices. The first EOF modes of rain gauge-measured and remote-sensed precipitation were almost identical (correlation +0.98, Table 7). Both modes were correlated positively with the NINO3 index (+0.28 and +0.33, respectively) and correlated negatively with the first EOF mode of wind (-0.43 and -0.46, respectively). Both time series reflect the strong El Niño event that occurred in 1997-1998, the La Niña that occurred during the second half of 1998 to early 2001, and the weak El Niño event of 2002-2003. The strong El Niño of 1997-98 also was reflected by a strong positive NINO3 index and a strong negative SOI index during this time period (Figure 9A, B). Maximum precipitation was observed in early 1998, during the 1997-1998 El Niño event, as indicated by strong positive values for the first EOF mode for precipitation during this time

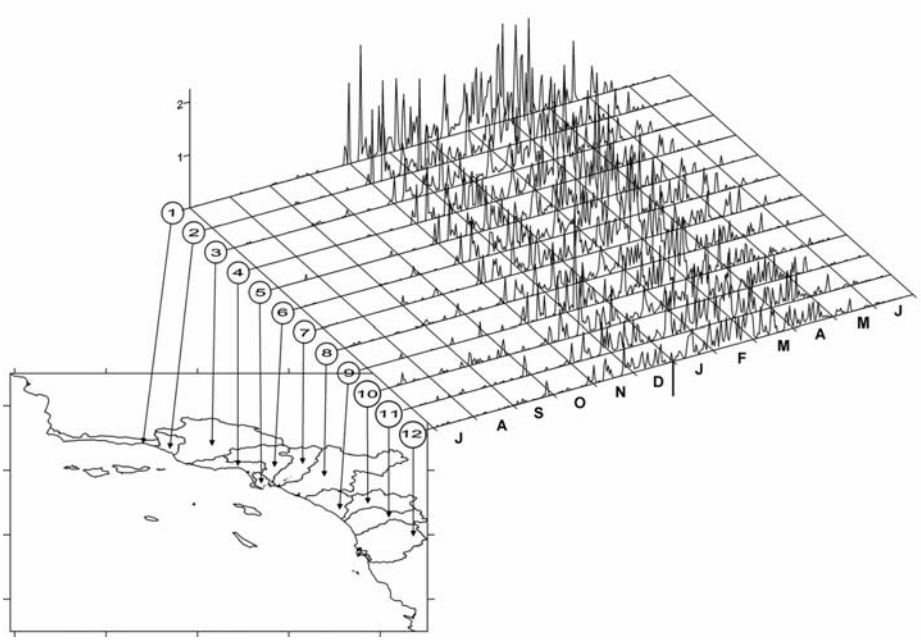

Figure 3. Seasonal patterns of rain gage-measured precipitation over different watersheds in southern California. X-axis represents months; numbers in circles along Y-axis indicate watersheds (Table 1); Z-axis represents mean daily precipitation (cm).

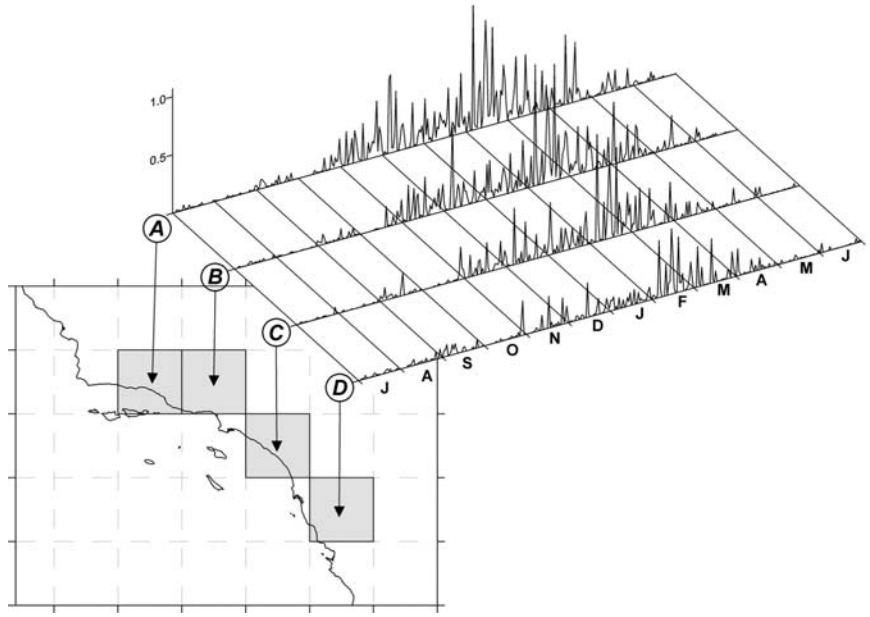

Figure 4. Seasonal patterns of remote-sensed precipitation in four 1ºx1º grid cells over southern California: 34º30'N, 119º30'W (A); 34º30'N, 118º30'W (B); 33º30'N, 117º30'W (C); 32º30'N, 116º30'W (D). X-axis represents months; Z-axis represents mean daily precipitation (cm).

(Figure 9C, E). Lower-than-normal winter season precipitation was observed in 1998-1999 and 2001-2002, corresponding with the La Niña event during this period. During these dry winter seasons, the first wind EOF mode was almost zero rather than negative as normal, indicating reduced moisture transport from the south (Figure 9G). The negative extremes of the second EOF mode of wind during these winter seasons (1998-1999 and 2001-2002) were more persistent than normal, indicating more consistent transport of dry continental air offshore (Figure 9H).

In contrast to the first EOF modes, the second EOF modes of remote-sensed and gauge-measured precipitation were not correlated, and their correla-

Table 4. The percentage of total variance of precipitation and wind explained by first three EOF modes.

Mode	Percent of variance (%)		
	Precipitation in rain gages	Remote-sensed precipitation	Wind
1	71.36	58.88	32.78
2	12.81	11.68	19.56
3	4.25	6.86	8.17

Table 5. Factor loadings of the first two EOF modes of rain gage precipitation. Mode 1 represents total rainstorm magnitude; Mode 2 north/south variability of rainstorms over southern California.

#	Watershed	Mode 1	Mode 2
1	Santa/ Barbara Creek	+0.659888	-0.544046
2	Ventura River	+0.863350	-0.047230
3	Santa Clara River	+0.885640	-0.324460
4	Santa Monica Bay	+0.896001	-0.318392
5	Dominguez Channel	+0.883535	-0.306208
6	Los Angeles River	+0.938702	-0.182517
7	San Gabriel River	+0.900198	-0.003092
8	Santa Ana River	+0.937154	+0.130448
9	San Juan Creek	+0.828604	+0.069477
10	Santa Margarita River	+0.763724	+0.515268
11	San Luis Rey River/Escondido Creek	+0.728664	+0.605077
12	San Diego River	+0.802439	+0.502018

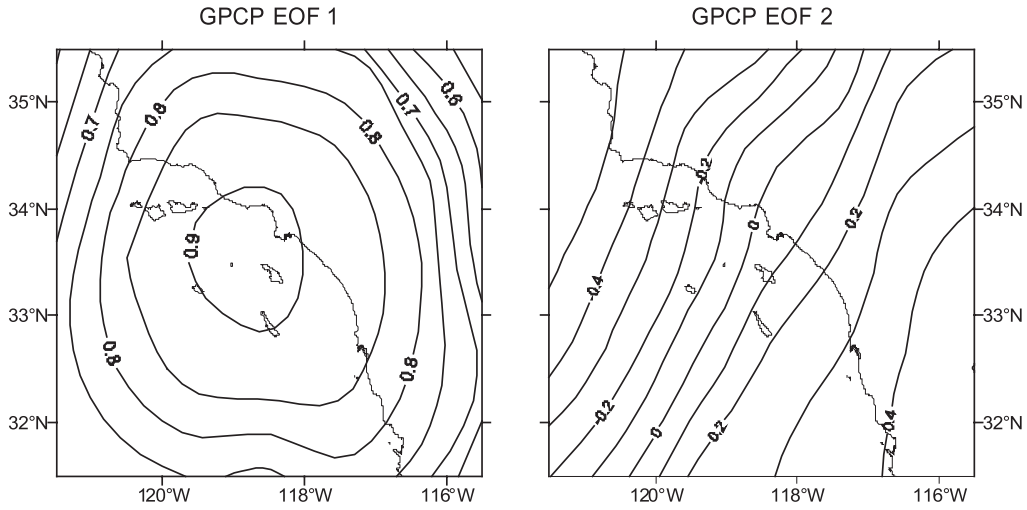

Figure 5. Graphic representation of first and second EOF modes of remote-sensed precipitation. The first EOF mode represents total precipitation, the second EOF mode represents the migration of the center of precipitation to the southeast.

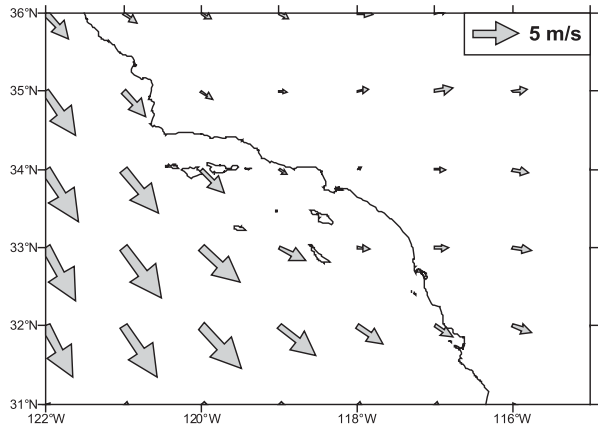

Figure 6. Wind speed averaged over the period of March 1997-October 2003. Larger arrows indicate higher wind speed.

tion with other parameters was also different. The second EOF mode of remote-sensed precipitation was not correlated to the SOI and NINO3 indices, but correlated to the first EOF mode of wind (+0.34). In contrast, the second EOF mode of the gauge-measured precipitation was correlated with SOI and NINO3 indices (-0.38 and +0.30, respectively), but not correlated with the wind EOF modes. The first and second EOF modes of rain gauge-measured precipitation were positively correlated (+0.36), but the two EOF modes of remote-sensed precipitation were not correlated.

The SOI index was correlated with the second EOF mode of rain gauge-measured precipitation (north/south variability in rain) and the second EOF mode of wind (south-southwesterly wind patterns) (-0.38 and -0.23, respectively). Neither the first EOF modes of wind and rain gauge-measured precipitation nor the EOF modes of remote-sensed precipitation were correlated with the SOI index.

Discussion

This study demonstrated that remote-sensed data of atmospheric precipitation accurately represent only the general large-scale (from seasonal to interannual) regional features of rain patterns in southern California and poorly represent local synoptic and spatial variability. At the daily time-scale, the correlation between the remote-sensed precipitation and the direct measurements of rainfall is weak (i.e., 0.3-0.5). However, the features of seasonal and interannual variability of precipitation can be derived from satellite observations with comparable reliability as from data measured by rain gauges. For example, at monthly and annual time scales, the correlation between the remote-sensed and rain gauge-measured precipitation is very high (>+0.90), indicating that the rainfall observations from space are most useful for the analysis of general climatological patterns of precipitation (Arkin and Ardanuy 1989). Finer scale analysis via remote sensing is limited by the spatial resolution of satellite data. Because satellite rainfall estimates are integrated over larger areas than rain gauge estimates, the absolute magnitudes at any particular location may be muted.

Low correlation between daily remote-sensed and gauge-measured precipitation can be explained by different temporal scales of these measurements. Remote-sensed patterns of atmospheric precipitation are based on one or a few snapshots of water vapor concentration. In contrast, rainfall data are accumulated in raingages over 24-h periods. As a result, the precipitation values in the grid cells of remote-sensed images are often far from the gauge-measured rainfall. These differences are illustrated by the rainstorm of March 14-17, 2003 (Figure 10). Both gauge-measured and remote-sensed data show that the zone of precipitation propagated from the

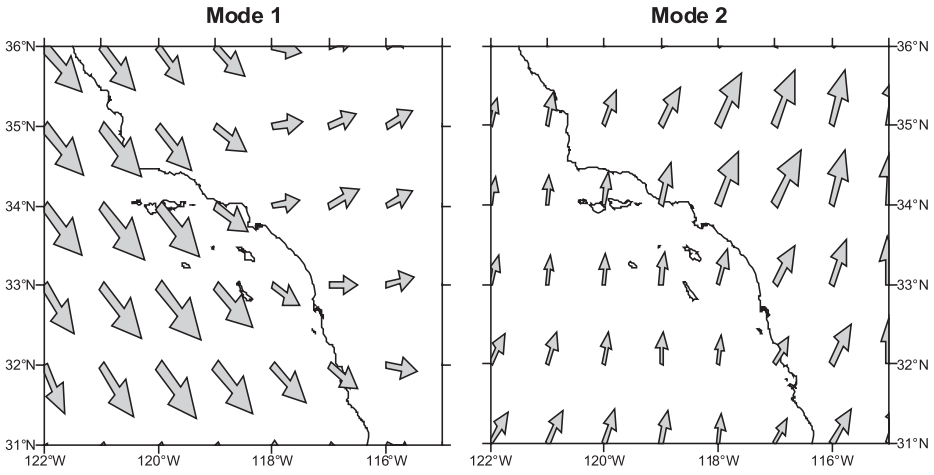

Figure 7. Graphic representation of first and second EOF modes of wind speed. Larger arrows indicate higher wind speed.

Table 6. Correlation between annually averaged (July-June) variations of precipitation in the watersheds of southern California and the remote-sensed precipitation in four locations during 1996-2003. In spite of small number of observations (N=7), all correlation coefficients are significant (p<0.05).

		A 34°30'N, 119°30'W	B 34°30'N, 118°30'W	C 33°30'N, 117°30'W	D 32°30'N, 116°30'W
1	Santa Barbara Creek	+0.9615	+0.9531	+0.9522	+0.9351
2	Ventura River	+0.9836	+0.9795	+0.9691	+0.9671
3	Santa Clara River	+0.9574	+0.9722	+0.9717	+0.9720
4	Santa Monica Bay	+0.9674	+0.9783	+0.9875	+0.9525
5	Dominguez Channel	+0.9829	+0.9845	+0.9878	+0.9629
6	Los Angeles River	+0.9801	+0.9892	+0.9852	+0.9800
7	San Gabriel River	+0.9751	+0.9533	+0.9457	+0.9128
8	Santa Ana River	+0.9849	+0.9909	+0.9877	+0.9747
9	San Juan Creek	+0.9619	+0.9893	+0.9931	+0.9830
10	Santa Margarita River	+0.9552	+0.9845	+0.9763	+0.9916
11	San Luis Rey River/Escondido Creek	+0.9840	+0.9909	+0.9785	+0.9865
12	San Diego River	+0.9812	+0.9947	+0.9839	+0.9913

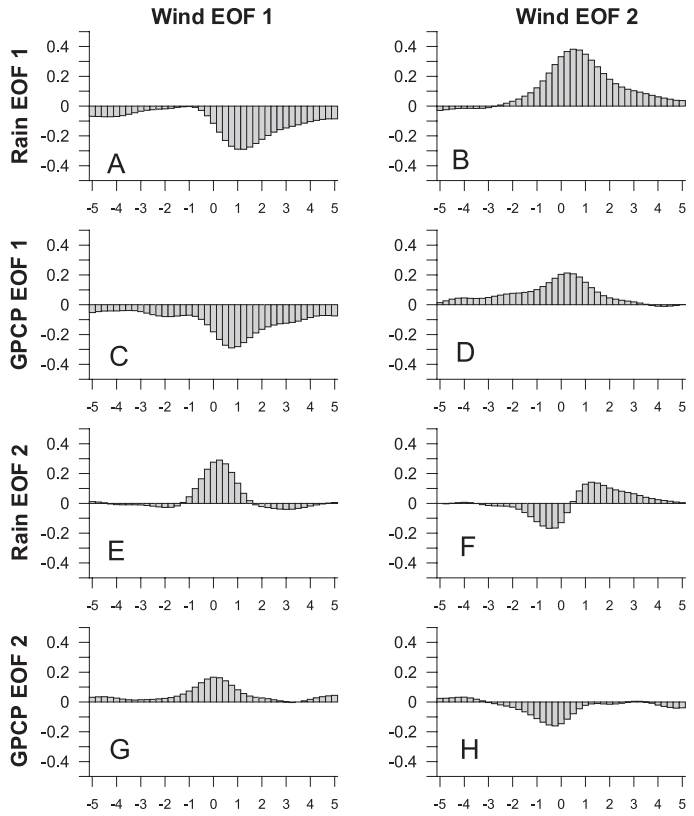

Figure 8. Time-lagged correlations between first two EOF modes of wind and the rain gage-measured (Rain) and remote-sensed (GPCP) precipitation. Positive time lag indicates that wind leads the precipitation.

west to the east. However, both types of data exhibit high levels of spatio-temporal variability; as a result, in each location of southern California, the precipitation measured by two methods was different, especially during the beginning (March 14; Figure 10 A, E) and at the end of the rainstorm (March 17; Figure 10 D, H).

Taking into account orographic effects on rainfall, we consider that gauge-measured and especially remote-sensed data do not adequately represent the precipitation patterns in the southern California watersheds. More than 60% of raingage stations were located within the elevation range 0-100 m (Figure 11A); at the same time, only 15% of the total area of 12 watersheds had elevation <100 m (Figure 11B). As for remote-sensed precipitation, 21.6% of the total area of the grid cells analyzed (see Figure 1) had elevation <100 m (Figure 11C), but most (16% of the total area) represented sea surface. Assuming that in southern California precipitation in elevated zones is higher than at the sea level, we concluded that the averaged figures of gauge-measured and especially remote-sensed precipitation data underestimate total rainfall over the watersheds.

The difference between the behavior of the second EOF modes of remote-sensed and gauge-measured precipitation (i.e., north-south migration of the rainstorms) is related to different spatial scales of these measurements. Wind patterns indicate that precipitation in southern California is regulated generally by atmospheric circulation patterns, which have been well documented in this area (Dorman 1982, Halliwell and Allen 1987, Dorman and Winant

Table 7. Correlations between monthly averaged SOI and NINO3 indices and EOF modes of rain gage-measured (Rain) and remote-sensed (GPCP) precipitation and wind. Only significant correlation coefficients ($p<0.05$) are given.

	NINO3	Rain EOF-1	Rain EOF-2	GPCP EOF-1	GPCP EOF-2	Wind EOF-1	Wind EOF-2
SOI	-0.77	-	-0.38	-	-	-	-0.23
NINO3	1.00	+0.28	+0.30	+0.33	-	-	-
Rain EOF-1	X	1.00	+0.36	+0.98	-	-0.43	-
Rain EOF-2	X	X	1.00	+0.32	-	-	-
GPCP EOF-1	X	X	X	1.00	-	-0.46	-
GPCP EOF-2	X	X	X	X	1.00	+0.34	-
Wind EOF-1	X	X	X	X	X	1.00	+0.34
Wind EOF-2	X	X	X	X	X	X	1.00

1995, Winant and Dorman 1997). The transport of atmospheric moisture is from the south-southwest. The gauge-measured precipitation included a relatively narrow zone of coastal watersheds (Figure 1); at the same time, the remote-sensed precipitation (see Figures 2 and 5) included the entire Southern California Bight and vast terrestrial areas. The variability of the second EOF mode of remote-sensed precipitation was correlated with the first EOF mode of wind only. We speculate that over the wide area including the Southern California Bight, strengthening of the dominating northwesterly wind decreases precipitation and shifts its center to the south (the second EOF mode of remote-sensed precipitation). The location of maximum rainfall in the coastal watersheds (the second EOF mode of the gauge-measured precipitation) did not change because the spatial scale of this zone is substantially smaller.

Both first EOF modes of remote-sensed and gauge-measured precipitations (total rainfall) were correlated with long-term, global-scale climatic NINO3 cycle. Maximum rainfall in the beginning of 1998 attributed to the 1997-1998 El Niño event, which was the strongest of the 20th century (McPhaden 1999). The correlation of remote-sensed precipitation with the NINO3 index was higher as compared with rain gauge-measured precipitation (Table 7); we attribute it to the fact that remote observations measure the water vapor concentration in the atmosphere rather than the exact amount of precipitated rainfall. Wind patterns in southern California did not change much during the El Niño period (Figure 9 G and H). However, the coincidence of El Niño and precipitation maxima in 1997-1998 and the correlation between the NINO3 index and the first EOF modes of both remote-sensed and gauge-measured precipitation indicate the influence of ENSO on the rainfall in southern California. Indeed, the warming of the surface ocean in the central equatorial Pacific (manifested in high NINO3 index) results in increased evaporation, accumulation of atmospheric moisture, and precipitation in the western U.S. coast including California.

The gauge-measured precipitation generally was higher than the remote-sensed precipitation, especially during the 1997-1998 extremely wet year (see Tables 2 and 3). This can be explained by the different size of the assessment sampling frames, wide in remote-sensed and narrow in gauge-measured data. Averaging over larger areas may result in the loss of substantial extremes, including increased rainfall related to ENSO cycle. The correlation between the rainfall in California and the ENSO cycle is not persistent but depends on the complex climatic processes centered in eastern Pacific. Not all previous studies concur with the relationships between ENSO and local rainfall that we observed in our data. Some studies have found evidence for an association between ENSO and California rainfall (Ramage 1975, Schonher and Nicholson 1989, Redmond and Koch 1991), while others reveal no clear ENSO modulation of California precipitation (Rasmusson and Wallace 1983, Ropelewski and Halpert 1986). Haston and Michaelsen (1994) reconstructed precipitation records from tree-ring data over several centuries and concluded that the probability of a wet year in California occurring during an ENSO is no greater than during a non-ENSO year; however, when wet years do occur during an ENSO, they are often extremely wet. The winter of 1997-1998 is an illustrative example of an extremely wet year. One potential explanation for the weak correlation between the ENSO cycle and precipitation observed by some researchers is that precipitation in

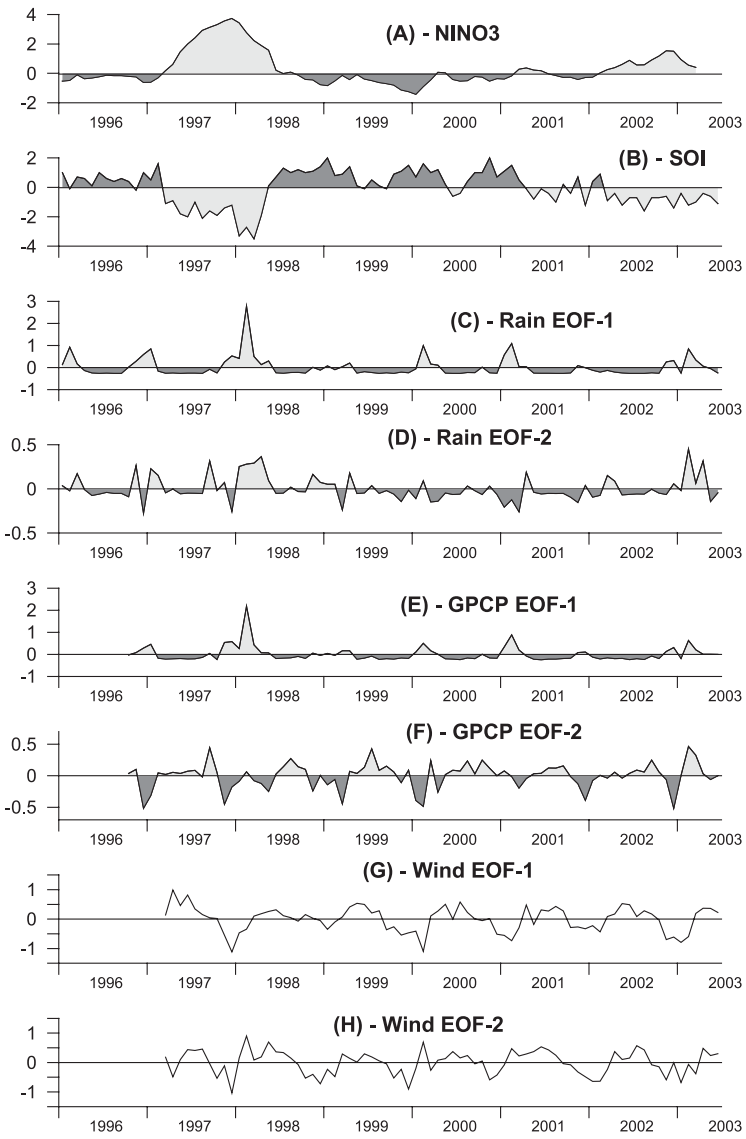

Figure 9. Monthly averaged NINO3 (A) and SOI (B) indices; first and second EOF modes of rain gage-measured precipitation (C and D); first and second EOF modes of remote-sensed precipitation (E and F); first and second leading EOF modes of wind (G and H).

California depends not only on accumulation of atmospheric moisture in the Pacific Ocean, but also on the pattern of atmospheric circulation transporting this moisture to North America. We speculate that during the winter of 1997-1998, the atmospheric circulation favored the transport of ENSO-influenced moisture to southern California. In contrast, during other years, the wind patterns were not as favorable. Recent studies support this hypothesis with their indication that the correlation between the ENSO cycle and precipitation in the western U.S. is better during periods when the SOI and NINO3 indices are significantly negatively correlated (McCabe and Dettinger 1999). NINO3 is based on sea surface temperature anomalies in the equatorial Pacific and is directly related to the intensity of evaporation and accumulation of moisture in the atmosphere. In contrast, SOI is based on the differences between atmospheric pressure in two distant locations and is more related to the pattern of atmospheric circulation. The negative correlation between SOI and NINO3 indicates that both evaporation and moisture transport influence precipitation over the west coast of the United States. During the early 1990s, this negative correlation was absent, resulting in less influence of ENSO on local rainfall (Ghil and Jiang 1998). In contrast, during our study period (1996-2003), this negative correlation was large (-0.77, Table 7), indicating a stronger influence of ENSO on local rainfall.

It is important to recognize the limitations on interpreting general climatic patterns of remote-sensed precipitation based on a relatively short period of data (eight years for this study). For example, when we compare the annual rain gauge-measured precipitation in 1996-2003 (Table 2) with long-term climatic data (Haston and Michaelsen 1994), we see that the precipitation during the wettest year of our observations (1997/1998) was comparable or even exceeded the highest values observed during six centuries of reconstructed data. At the same time, the precipitation observed during the driest year (2001/2002) was also substantially higher than that of the driest years of the historical data (Haston and Michaelsen 1994). At the same time, the range of variability of remote-sensed precipitation (Table 3) is within the range of historical data. The possible cause of this difference is a coarser spatial resolution of the remote-sensed dataset. Also, the uniformly high gauge-measured precipitation values can be explained by a "warm" PDO phase, which started in 1976-1977, when sea surface temperature in the northeastern Pacific was warmer (Mantua et al. 1997, Parrish et al. 2000) and the El Niño events were enhanced (Gershunov and Barnett 1998). Inman and Jenkins (1999) indicate

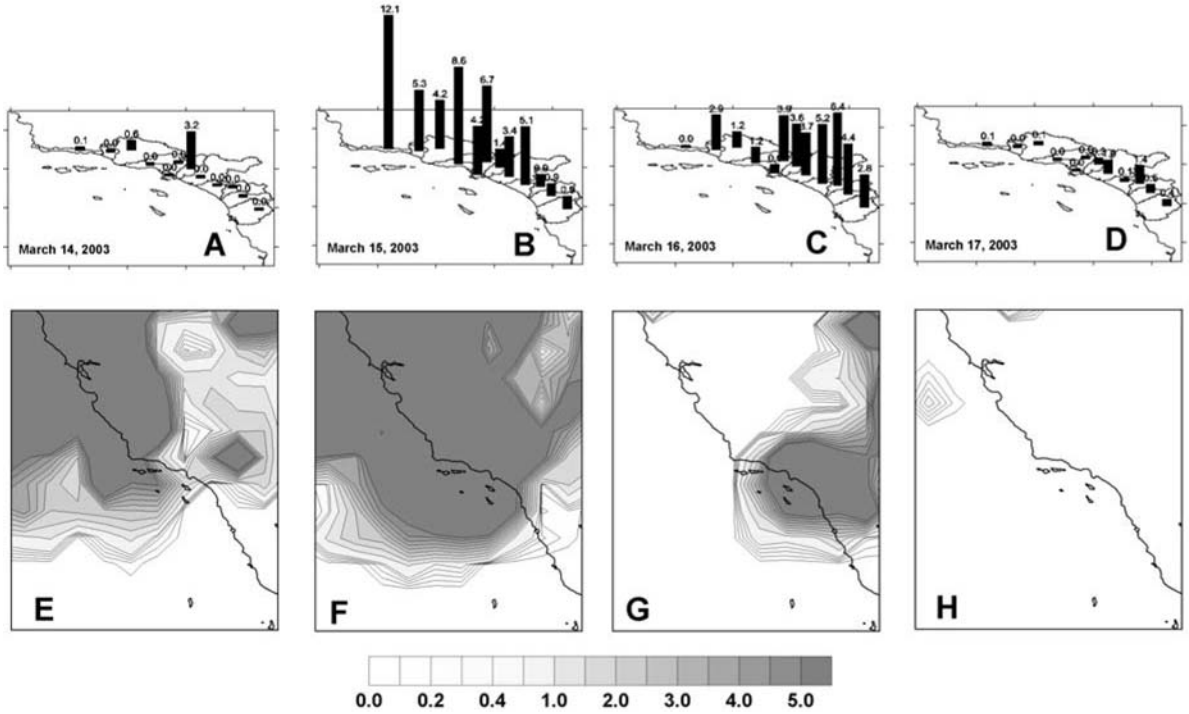

Figure 10. Gauge-measured precipitation in southern California (A-March 14; B-March 15; C-March 16; D-March 17, 2003) and remote-sensed precipitation in central and southern California (E- March 14; F-March 15; G-March 16; H-March 17, 2003) (cm/day).

that the climate in central and southern California became wetter after 1968 (after 1977 in the watersheds to the south of San Luis Rey) and have been characterized by more frequent and extensive floods (related to ENSO) than during the previous dry period. We speculate that the increase of rainfall in southern California was associated with the global climate shift in 1976-1977, which influenced the ecosystems all over the world (Walther et al. 2002). Whether the PDO is shifting from a warm phase back to a cold phase is currently an open question. When the 1998-1999 El Niño event changed to very strong La Niña, some scientists declared that the "warm" PDO phase is over and the "cold" phase started (Bograd and Lynn 2003, Chavez et al. 2003, McGowan et al. 2003). To make a definite conclusion, we need at least a decade of future observations. Consequently, development of statistical relationships must be revisited as our understanding of long-term climate trends continues to increase.

This study illustrates that statistical analysis of both remote-sensed and field-measured precipitation data can provide valuable insight into the mechanisms and forcing functions behind previously observed spatial and temporal patterns of wind and rainfall. These quantitative relationships provide a critical foundation for development of predictive models of relationships between climatic patterns and coastal water quality. For example, Inman and Jenkins (1999) analyzed the effect of El Niño storms on sediment flux by rivers in southern and central California and found significant relationships between climate patterns, stream flow, and sediment discharge. It is reasonable to assume that similar relationships occur for pollutants (especially those typically bound to sediments). The ability to model the effect of climatic patterns on pollutant discharge to the coast will greatly enhance management of coastal water quality. Daily remote-sensed rainfall data produced at GPCP can be used in these studies, but for large-scale assessments only (e.g., interannual variability of freshwater and pollutants discharge along the entire coast of southern California). To analyze the spatial details of this process, we should either use rain gage-measured data or obtain remote-sensed observations of higher frequency and finer resolution.

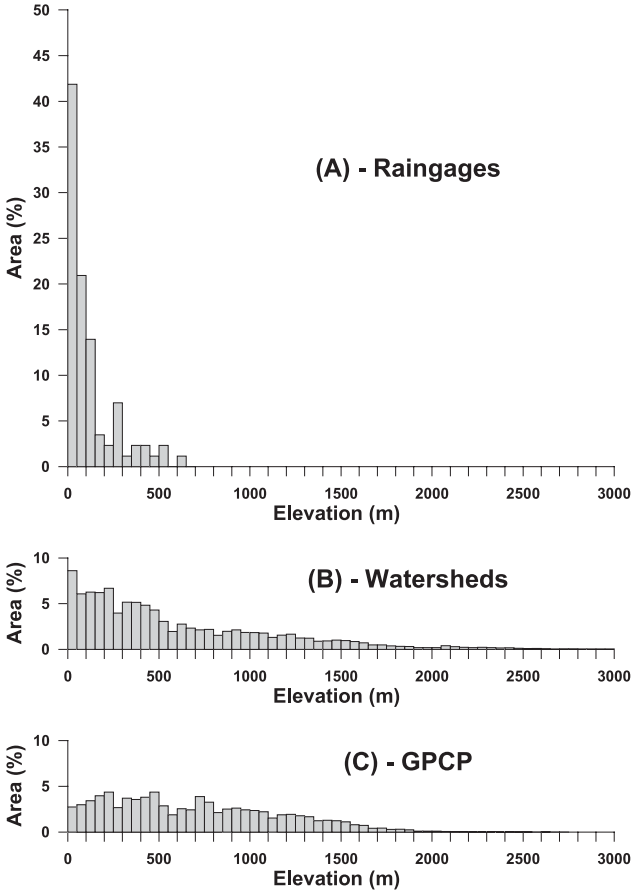

Figure 11. Elevation of the 98 rain-gauge stations (A), in all 12 watersheds (B), and in the four rectangles where remote-sensed precipitation was measured (C).

Literature Cited

Ackerman, D., K.C. Schiff and S.B. Weisberg. In press. Evaluating HSPF in an arid, urbanized watershed. *Journal of American Water Resources Association*.

Arkin, P.A. and P.E. Ardanuy. 1989. Estimating climatic-scale precipitation from space: A review. J*ournal of Climate* 2: 1229-1238.

Bailey, H.P. 1966. The climate of southern California. University of California Press. Berkeley, CA.

Beuhler, M. 2003. Potential impacts of global warming on water resources in southern California. *Water Science and Technology* 47: 165-168.

Bograd, S.J. and R.J. Lynn. 2003. Long-term variability in the Southern California Current System. *Deep-Sea Research II* 50: 2355-2370.

Chavez, F.P., J. Ryan, S.E. Lluch-Cota and M.C. Niquen. 2003. From anchovies to sardines and back: Multidecadal change in the Pacific Ocean. *Science* 299: 217-221.

Dorman, C.E. 1982. Winds between San Diego and San Clemente Island. *Journal of Geophysical Research* 87: 9636-9646.

Dorman, C.E. and C.D. Winant. 1995. Buoy observations of the atmosphere along the west coast of the United States. *Journal of Geophysical Research* 100: 16029-16044.

Gershunov, A. and T.P. Barnett. 1998. Interdecadal modulation of ENSO teleconnections. *Bulletin of the American Meteorological Society* 79: 2715-2725.

Ghil, M. and N. Jiang. 1998. Recent forecast skill for the El Niño/Southern Oscillation. *Geophysical Research Letters* 25: 171-174.

Halliwell, G.R. and J.S. Allen. 1987. The large-scale coastal wind field along the west coast of North America. *Journal of Geophysical Research* 92: 1861-1884.

Haston, L. and J. Michaelsen. 1994. Long-term central coastal California precipitation variability and relationship to El Niño-Southern Oscillation. *Journal of Climate* 7: 1373-1387.

Huffman, G.J., R.F. Adler, M.M. Morrissey, D.T. Bolvin, S. Curtis, R. Joyce, B. McGavock and J. Susskind. 2002. Global precipitation at one-degree daily resolution from multisatellite observations. *Journal of Hydrometeorology* 2: 36-50.

Inman, D.L. and S.A. Jenkins. 1999. Climate change and the episodicity of sediment flux of small California rivers. *Journal of Geology* 107: 251-270.

Lu, R., R.P. Turco, K. Stolzenbach, S.K. Friedlander, C. Xiong, K. Schiff, L. Tiefenthaler and G. Wang. 2003. Dry deposition of airborne trace metals on the Los Angeles Basin and adjacent coastal waters. *Journal of Geophysical Research* 108: 4074, doi:4010.1029/2001JD001446.

Mantua, N.J., S.R. Hare, Y. Zhang, J.M. Wallace and R.C. Francis. 1997. A Pacific Interdecadal Climate Oscillation with impacts on salmon production. *Bulletin of the American Meteorological Society* 78: 1069-1079.

McCabe, G.J. and M.D. Dettinger. 1999. Decadal variations in the strength of ENSO teleconnections with precipitation in the western United States. *International Journal of Climatology* 19: 1399-1410.

McGowan, J.A., S.J. Bograd, R.J. Lynn and A.J. Miller. 2003. The biological response to the 1977 regime shift in the California Current. *Deep-Sea Research II* 50: 2567-2582.

McPhaden, M.J. 1999. Genesis and evolution of the 1997-98 El Niño. *Science* 283: 950-954.

Mount, J.F. 1995. California Rivers and Streams: The Conflict Between Fluvial Process and Land Use. University of California Press. Berkeley, CA.

Parrish, R.H., F.B. Schwing and R. Mendelssohn. 2000. Mid-latitude wind stress: the energy source for climatic shifts in the North Pacific Ocean. *Fisheries Oceanography* 9: 224-238.

Priesendorfer, R.W. 1988. Principle Component Analysis in Meteorology and Oceanography. Elsevier Science. New York, NY.

Ramage, C.S. 1975. Preliminary discussion of the meteorology of the 1972-1973 El Niño. *Bulletin of the American Meteorological Society* 56: 234-242.

Rasmusson, E.M. and J.M. Wallace. 1983. Meteorological aspects of El Niño/Southern Oscillation. *Science* 222: 1195-1201.

Redmond, K.T. and R.W. Koch. 1991. Surface climate and streamflow variability in the western United States and their relationship to large-scale circulation indices. *Water Resources Research* 27: 2381-2399.

Ropelewski, C.F. and M.S. Halpert. 1986. North American precipitation and temperature patterns associated with the El Niño/Southern Oscillation (ENSO). *Monthly Weather Review* 114: 2352-2362.

Schonher, T. and S.E. Nicholson. 1989. The relationship between California rainfall and ENSO events. *Journal of Climate* 2: 1258-1269.

Tiefenthaler, L.L. and K.C. Schiff. 2003. Effects of rainfall intensity and duration on first flush of stormwater pollutants. pp. 209-215 in: S.B. Weisberg and D. Elmore (eds.), Southern California Coastal Water Research Project Annual Report 2001-2002. Westminster, CA.

Vaze, J. and F.H.S. Chiew. 2003. Study of pollutant washoff from small impervious experimental plots. *Water Environment Research* 39: 1160-1169.

Walther, G.-R., E. Post, P. Convey, A. Menzel, C. Parmesan, T.J.C. Beebee, J.-M. Fromentin, O. Hoegh-Guldberg and F. Bairlein. 2002. Ecological responses to recent climate change. *Nature* 416: 389-395.

Ward, A.D. and W.J. Elliot. 1995. Environmental Hydrology. CRC Press. Boca Raton, FL.

Winant, C.D. and C.E. Dorman. 1997. Seasonal patterns of surface wind stress and heat flux over the Southern California Bight. *Journal of Geophysical Research* 102: 5641-5653.

Acknowledgements

The authors thank the Global Precipitation Climatology Project (GPCP) for remote-sensed precipitation data, the NOAA National Data Center Climate Data Online (NNDC/CDO) for the rain gauge-measured precipitation data, the National Center for Environmental Prediction (NCEP) and the NASA Goddard Space Flight Center Distributed Active Archive Center (GSFC DAAC) for the global wind data. We thank S.B. Weisberg for critical discussion of the results. Critical remarks by G. Robertson and an unknown reviewer are very appreciated and helped to improve this paper substantially.

Appendix A. Rain gage stations in the watersheds (WS) of southern California. NCDC - National Climate Data Center Cooperative Station Number; WBAN - Weather Bureau, Army, and Navy Station Number; Cnt - county, Lat, Lon - station coordinates, H - elevation (m above sea level).

WS	NCDC	WBAN	Cnt	Lat (N)	Lon (W)	H (m)	Station Name
01 Santa	47902		SB	34.417	119.683	0.5	SANTA BARBARA
Barbara	47905	23190	SB	34.433	119.850	0.8	SANTA BARBARA MUNICIPAL AP
02 Ventura	46399		VE	34.467	119.250	66.0	OJAI
	49285		VE	34.283	119.300	9.7	VENTURA
03 Santa	40014		LA	34.500	118.267	275.9	ACTON ESCONDIDO FC261
Clara	42941		LA	34.700	118.433	284.3	FAIRMONT
	46161		LA	34.400	118.600	164.0	NEWHALL 5 NW
	46162		LA	34.383	118.533	115.5	NEWHALL S FC32CE
	46165		LA	34.367	118.566	130.1	NEWHALL
	47735	23187	LA	34.750	118.717	419.0	SANDBERG
	48014		LA	34.583	118.450	195.6	SAUGUS POWER PLANT 1
	49345		LA	34.483	118.133	291.2	VINCENT FS FC 120
	46569		VE	34.200	119.183	4.5	OXNARD
	46572		VE	34.217	119.133	5.8	OXNARD WSFO
	46940		VE	34.400	118.750	67.8	PIRU 2 ESE
	47957		VE	34.317	119.133	22.0	SANTA PAULA
04 Santa	42214		LA	34.000	118.417	5.1	CULVER CITY
Monica Bay	44867		LA	34.083	118.883	148.6	LECHUZA PTRL ST FC352B
	43392		LA	34.083	118.483	102.5	GETTY CENTER
	46663		LA	33.800	118.383	20.1	PALOS VERDES EST FC43D
	47953		LA	34.000	118.500	1.3	SANTA MONI PIER
	48967		LA	34.083	118.600	69.2	TOPANGA PATROL STN FC6
	49152		LA	34.067	118.450	40.0	U C L A
05 Dominguez Channel	45114	23174	LA	33.933	118.383	9.0	LOS ANGELES INTL ARPT
	48973	03122	LA	33.800	118.333	10.2	TORRANCE MUNICIPAL ARPT
06 Los	40144		LA	34.183	118.133	104.7	ALTADENA
Angeles	40798		LA	34.300	118.183	215.2	BIG TUJUNGA DAM FC46DE
River	41194		LA	34.183	118.350	60.8	BURBANK VALLEY PUMP PLANT
	41484		LA	34.183	118.567	73.4	CANOGA PARK PIERCE COLLEGE
	42494		LA	33.933	118.150	10.2	DOWNEY FIRE STN FC107D
	44628		LA	34.217	118.250	145.4	LA CRESCENTA FC 251C
	45115	93134	LA	34.050	118.233	21.4	LOS ANGELES CVC CNTR
	45790		LA	34.017	118.100	22.3	MONTEBELLO
	46006		LA	34.233	118.067	532.6	MT WILSON NO 2
	46263		LA	34.233	118.533	79.6	NORTHRIDGE CAL STATE
	46602		LA	34.333	118.400	139.3	PACOIMA DAM FC 33 A-E
	46719		LA	34.150	118.150	80.2	PASADENA
	47785		LA	34.100	118.100	41.8	SAN GABRIEL FIRE DEPT
07 San	42090		LA	34.100	117.883	54.2	COVINA CITY YRD FC387B
Gabriel	42198		LA	34.317	117.833	498.9	CRYSTAL LAKE FC 283 C
	43452		LA	34.150	117.850	85.5	GLENDORA FC 287B
	45085	23129	LA	33.817	118.150	2.9	LONG BEACH DAUGHERTY FLD
	47050		LA	34.083	117.767	96.6	POMONA L POLY
	47749		LA	34.100	117.800	88.7	SAN DIMAS FIRE FC95
	47776		LA	34.150	117.900	69.1	SAN GABRIEL NYON P H
	47779		LA	34.200	117.867	137.6	SAN GABRIEL DAM FC425B
	49431		LA	34.000	117.867	45.3	WALNUT NI FC102C
	49660		LA	33.983	118.017	39.0	WHITTIER CITY YD FC106C
08 Santa	40192		OR	33.867	117.850	31.1	ANAHEIM
Ana River	46175	03107	OR	33.6	117.883	0.9	NEWPORT BEACH
	47888		OR	33.750	117.867	12.5	SANTA ANA FIRE STATION
	49087		OR	33.700	117.750	21.8	TUSTIN IRVINE RANCH
	49847		OR	33.883	117.817	32.5	YORBA LINDA
	40609	23156	RI	33.933	116.967	241.5	BEAUMONT 1 E
	42805		RI	33.667	117.333	119.4	ELSINORE

Appendix A. (continued)

	47470		RI	33.950	117.383	78.0	RIVERSIDE FIRE STA 3
	47473		RI	33.967	117.367	91.6	RIVERSIDE CITRUS EXP STN
	40741		SB	34.250	116.900	628.0	BIG BEAR LAKE
	45218		SB	34.233	117.467	253.6	LYTLE CREEK R S
	47306		SB	34.050	117.183	122.4	REDLANDS
	47723		SB	34.133	117.250	105.9	SAN BERNARDINO F S 226
09 San	44647		OR	33.550	117.783	3.3	LAGUNA BEACH
Juan	47836		OR	33.533	117.550	34.8	SAN JUAN CANYON
10 Santa	46319		SD	33.383	116.800	255.5	OAK GROVE R S
Margarita	46377		SD	33.217	117.400	0.9	OCEANSIDE MARINA
	46657		SD	33.383	116.833	515.6	PALOMAR MOUNTAIN OBSERV.
	40235		RI	33.550	116.667	363.7	ANZA
11 San Luis	42863		SD	33.117	117.083	55.7	ESCONDIDO NO 2
Rey/	43914		SD	33.233	116.767	250.8	HENSHAW DAM
Escondido	49378		SD	33.233	117.233	47.4	VISTA 2 NNE
12 San	40136		SD	32.833	116.767	161.2	ALPINE
Diego	41758		SD	32.633	117.083	5.2	CHULA VISTA
	42239		SD	32.983	116.583	431.1	CUYAMACA
	42406		SD	32.850	116.617	325.2	DESCANSO RANGER STN
	42706		SD	32.817	116.983	37.6	EL CAJON
	42709		SD	32.883	116.817	55.7	EL CAPITAN DAM
	44412		SD	33.083	116.600	391.6	JULIAN CDF
	44710		SD	32.850	116.900	64.1	LAKESIDE 2 E
	44735		SD	32.767	117.017	49.2	LA MESA
	47111		SD	33.017	117.033	60.2	POWAY VALLEY
	47228		SD	33.017	116.900	136.6	RAMONA FIRE DEPT
	47740	23188	SD	32.733	117.183	1.4	SAN DIEGO LINDBERGH FIELD
	47741		SD	32.767	117.233	1.4	SAN DIEGO SEAWORLD
	47874		SD	33.100	117.000	39.0	SAN PASQUAL ANIMAL PK
		93107	SD	32.867	117.133	42.6	SAN DIEGO MIRAMAR NAS
		93112	SD	32.700	117.200	4.5	SAN DIEGO NORTH ISLAND NAS